J|A|C|S ARTICLES

Published on Web 12/14/2009

Probing Molecular Motion by Double-Quantum (^{13}C,^{13}C) Solid-State NMR Spectroscopy: Application to Ubiquitin

Robert Schneider,[†] Karsten Seidel,[†,§] Manuel Etzkorn,[†,||] Adam Lange,[†] Stefan Becker,[†] and Marc Baldus*[,‡]

Department for NMR-based Structural Biology, Max-Planck-Institute for Biophysical Chemistry, Am Fassberg 11, 37077 Göttingen, Germany, and Bijvoet Center for Biomolecular Research, Utrecht University, Padualaan 8, 3584 CH Utrecht, The Netherlands

Received July 29, 2009; E-mail: m.baldus@uu.nl

Abstract: We demonstrate the use of two-dimensional (^{13}C,^{13}C) double-quantum spectroscopy to detect molecular dynamics by solid-state NMR. Data collected on tyrosine-ethylester (TEE) are in line with previously determined (^{1}H,^{13}C) order parameters. Application of these experiments to microcrystalline ubiquitin reveals the presence of dynamics on millisecond or faster time scales and differences in local mobility depending on microcrystal preparation. In addition, solid-state NMR-based structure calculation indicates conformational variability of loop regions between different solid-phase ubiquitin preparations. Our data relate preparation-dependent changes observed in NMR spectral parameters such as chemical shifts and through-space correlations to differences in ubiquitin dynamics and conformation and suggest a prominent role of molecular mobility in microcrystalline ubiquitin.

Introduction

Molecular motion is of fundamental relevance for protein function. It constitutes the source of protein conformational entropy and is crucially involved in governing protein−protein interactions.[1] Nuclear magnetic resonance (NMR) spectroscopy is a method ideally suited to measure protein dynamics over a wide range of time scales in solution and in the solid state.[2−5] Solid-state NMR (ssNMR) has long been used to study molecular motion in applications ranging from small molecules and polymers to biomolecules.[3,6−9] In addition to relaxation-based analyses,[3,8,10−14] the effect of molecular motion upon anisotropic parameters such as the quadrupolar coupling or the one-bond (^{1}H,^{13}C/^{15}N) dipolar coupling has been used to probe dynamics in the solid state.[7−9,15−17] Molecular motion also impacts homonuclear dipolar couplings, as has been demonstrated using (^{1}H,^{1}H) correlation spectroscopy to measure motion and the supramolecular organization of polymers.[18−20] Because of the limited spectral resolution, such methods are, however, of limited use for larger biomolecules, which, on the other hand, can often be readily prepared in isotope-labeled form.

Here, we demonstrate the utility of (^{13}C,^{13}C) double-quantum (2Q) spectroscopy to detect molecular motion in fully isotope-labeled biomolecules. This approach offers the opportunity to detect modes of motion complementary to those covered by measuring (^{1}H,^{13}C/^{15}N) couplings, in the high spectral resolution afforded by ^{13}C ssNMR spectroscopy. First, we developed a motional analysis of (^{13}C,^{13}C) 2Q ssNMR data on L-tyrosine-ethylester (TEE), which has been shown to exhibit molecular motion in the solid state.[17,21−23] We then applied 2Q spectroscopy to the 76-residue protein ubiquitin, an established system for studies of protein structure and dynamics by solution- and

[†] Max-Planck-Institute for Biophysical Chemistry.
[‡] Utrecht University.
[§] Current address: Polymer Physics (GKP/R), BASF SE, 67056 Ludwigshafen, Germany.
[||] Current address: Harvard Medical School, Department of Biological Chemistry and Molecular Pharmacology, 240 Longwood Ave., Boston, MA 02115.

(1) Smock, R. G.; Gierasch, L. M. *Science* **2009**, *324*, 198–203.
(2) Peng, J.; Wagner, G. *Methods Enzymol.* **1994**, *239*, 563–596.
(3) Palmer, A. G.; Williams, J.; McDermott, A. *J. Phys. Chem.* **1996**, *100*, 13293–13310.
(4) Frederick, K. K.; Marlow, M. S.; Valentine, K. G.; Wand, A. J. *Nature* **2007**, *448*, 325–U3.
(5) Lange, O. F.; Lakomek, N. A.; Fares, C.; Schröder, G. F.; Walter, K. F. A.; Becker, S.; Meiler, J.; Grubmüller, H.; Griesinger, C.; de Groot, B. L. *Science* **2008**, *320*, 1471–1475.
(6) Spiess, H. W. *Chem. Phys.* **1974**, *6*, 217–225.
(7) Griffin, R. G. *Methods Enzymol.* **1981**, *72*, 108–174.
(8) Torchia, D. A. *Annu. Rev. Biophys. Bioeng.* **1984**, *13*, 125–144.
(9) Opella, S. J. *Methods Enzymol.* **1986**, *131*, 327–61.
(10) Cole, H. B. R.; Torchia, D. A. *Chem. Phys.* **1991**, *158*, 271–281.
(11) Giraud, N.; Böckmann, A.; Lesage, A.; Penin, F.; Blackledge, M.; Emsley, L. *J. Am. Chem. Soc.* **2004**, *126*, 11422–11423.
(12) Chevelkov, V.; Diehle, A.; Reif, B. *J. Chem. Phys.* **2008**, *128*, 052316.
(13) Ader, C.; Pongs, O.; Becker, S.; Baldus, M. *Biochim. Biophys. Acta: Biomembr.*, doi:10.1016/j.bbamem.2009.06.023.
(14) Cady, S. D.; Hong, M. *Proc. Natl. Acad. Sci. U.S.A.* **2008**, *105*, 1483–1488.
(15) Schmidt-Rohr, K.; Spiess, H. W. *Multidimensional Solid-State NMR and Polymers*; Academic Press: London, 1994.
(16) Huster, D.; Xiao, L.; Hong, M. *Biochemistry* **2001**, *40*, 7662–7674.
(17) Seidel, K.; Etzkorn, M.; Sonnenberg, L.; Griesinger, C.; Sebald, A.; Baldus, M. *J. Phys. Chem. A* **2005**, *109*, 2436–2442.
(18) Graf, R.; Demco, D. E.; Hafner, S.; Spiess, H. W. *Solid State Nucl. Magn. Reson.* **1998**, *12*, 139–152.
(19) Gasper, L.; Demco, D. E.; Blümich, B. *Solid State Nucl. Magn. Reson.* **1999**, *14*, 105–116.
(20) Schnell, I.; Spiess, H. W. *J. Magn. Reson.* **2001**, *151*, 153–227.
(21) Helluy, X.; Sebald, A. *J. Phys. Chem. B* **2003**, *107*, 3290–3296.
(22) Raleigh, D. P.; Creuzet, F.; Gupta, S. K. D.; Levitt, M. H.; Griffin, R. G. *J. Am. Chem. Soc.* **1989**, *111*, 4502–4503.
(23) Frydman, L.; Vallabhaneni, S.; Lee, Y. K.; Emsley, L. *J. Chem. Phys.* **1994**, *101*, 111–117.

solid-state NMR.[24−29] SsNMR studies in ubiquitin and other microcrystalline proteins have revealed that the details of the preparation of protein microcrystals can influence NMR spectral parameters.[24,30,31] Chemical-shift variations between different microcrystalline preparations and with respect to solution-state NMR assignments have been reported,[24] as well as the absence of through-space correlation signals expected from a reference single-crystal structure.[32] These cases often involved protein regions known to exhibit increased dynamics in solution. Thus, a more detailed insight into protein dynamics in the microcrystalline state and its dependence on sample preparation is highly desirable.

In this work, we have investigated solid-phase ubiquitin after precipitation using poly(ethylene glycol) (PEG). In this microcrystalline state, we previously found preparation-dependent chemical-shift variations in putatively mobile protein regions.[24] Moreover, we here uncovered protein regions in which through-space polarization transfer is significantly less efficient than expected from the ubiquitin crystal structure. To investigate whether these findings are related to molecular mobility, we have determined dipolar (^{13}C,^{13}C) order parameters from (2Q,1Q) correlation spectroscopy and compared them to available dynamical data for microcrystalline ubiquitin using 2-methyl-2,4-pentanediol (MPD) as precipitation agent.[25,26] Effects of protein conformation were probed using an automated structure calculation procedure.[33,34] Our results demonstrate the sensitivity of 2Q ssNMR spectroscopy for residue-specific molecular motion in proteins up to the millisecond (ms) time scale and relate preparation-dependent chemical-shift changes to local differences in dynamics and conformation.

Materials and Methods

Sample Preparation. A dilute sample of L-tyrosine-ethylester (TEE) was prepared as described in ref 17 by dissolving 4.5 mg of uniformly ^{13}C-labeled TEE and 45 mg of TEE with ^{13}C in natural abundance in ethanol. After overnight evaporation of the solvent, the sample was ground and dried in a vacuum desiccator prior to transfer to a standard 4 mm magic-angle-spinning (MAS)[35] rotor.

Uniformly [^{13}C,^{15}N]-labeled, PEG-precipitated microcrystalline ubiquitin (further denoted as Ubi-P) was prepared as described in ref 24. The protein was expressed recombinantly in *E. coli* and purified by established procedures.[36,37] Subsequently, it was freeze-dried, precipitated from poly(ethylene glycol) as described in refs 30, 31, and transferred to a 4 mm MAS rotor. The sample quantity was about 8 mg.

Solid-State NMR. NMR experiments were conducted using 4 mm triple-resonance (^{1}H, ^{13}C, ^{15}N) MAS probes (Bruker Biospin, Karlsruhe, Germany) at static magnetic fields of 9.4, 14.1, and 18.8 T corresponding to 400, 600, and 800 MHz proton resonance frequencies, respectively. 2D (2Q,1Q) correlation spectra on TEE were recorded at a static field of 9.4 T, using 7.8 kHz MAS and a sample temperature of about 0 °C. After cross-polarization (CP) using a contact time of 1 ms and radiofrequency (rf) field strengths of 50 and 58 kHz on ^{13}C and ^{1}H, respectively, the SPC5 pulse sequence[38] was used for generation of 2Q coherence, with a ^{13}C rf field strength of 35 kHz and 2Q excitation and reconversion times varying between 154 and 1436 μs. ^{1}H field strength during 90° pulses and SPINAL64 proton decoupling[39] was 86 kHz. 180 and 1280 acquisition data points with dwell times of 10 and 32 μs were recorded in indirect and direct dimensions, respectively. (2Q,1Q) correlation spectra of ubiquitin were recorded at a static field of 18.8 T and 8 kHz MAS frequency. The effective sample temperature (calibrated using nickelocene[40]) was +17 °C, as in experiments for determination of (^{1}H,^{13}C) order parameters on Ubi-M.[26] SPC5 2Q excitation and reconversion times each of 250, 500, 750, or 1000 μs at a ^{13}C field strength of 40 kHz were used. A ^{1}H field strength of 83 kHz was used for 90° pulses and SPINAL64 decoupling, except during 2Q excitation and reconversion, where the decoupling field strength was set to 90 kHz. (2Q,1Q) spectra were recorded with 240 and 1280 acquisition data points in indirect and direct dimensions, using dwell times of 18.75 and 8 μs, respectively. CHHC[41,42] spectra were recorded at 14.1 T using short CPs (80 μs) bracketing (^{1}H,^{1}H) mixing, and (^{1}H,^{1}H) mixing times of 62.5, 125, 180, and 250 μs, with 170 acquisition data points (dwell time 40 μs) in the indirect and 1024 (dwell time 10 μs) in the direct dimension. MAS frequency was set to 11 kHz, and effective sample temperature was +5 °C. ^{1}H field strengths were 83 kHz for 90° pulses and 72 kHz for SPINAL64 decoupling. All spectra were processed in XWinNMR or Topspin (Bruker Biospin, Karlsruhe, Germany), using 1024 × 1024 processing data points (2048 × 4096 for ubiquitin (2Q, 1Q) spectra) and a QSINE window function, and analyzed in SPARKY (T. D. Goddard and D. G. Kneller, SPARKY 3, University of California, San Francisco).

CHHC and Chemical Shift Analysis. For analysis of CHHC spectra, the software MOLMOL[43] was used to add protons to the ubiquitin crystal structure (Protein Data Bank (PDB) entry 1UBQ) and to list all (^{1}H,^{1}H) pairs spaced no more than 2.7 or 3.5 Å apart (for analysis of CHHC spectra with 62.5 or 180 μs mixing time, respectively). Cross-peak predictions were then obtained from assignments for ^{13}C nuclei bound to these protons, using assignments for 86% of the Ubi-P sequence as published in ref 24. The resultant correlations were considered as expected correlations, and percentages for present or absent cross-peaks assume these sets as 100% values. Hence, only (^{13}C,^{13}C) correlations involving nuclei that were both assigned in Ubi-P could be probed. A cross-peak was considered present in the spectrum if spectral intensity was found within 0.2 ppm around its predicted position on at least one side of the diagonal, using a lower contour threshold of 2.3 times the spectral noise level as determined by SPARKY.

(24) Seidel, K.; Etzkorn, M.; Heise, H.; Becker, S.; Baldus, M. *ChemBioChem* **2005**, *6*, 1638–1647.
(25) Zech, S. G.; Wand, A. J.; McDermott, A. E. *J. Am. Chem. Soc.* **2005**, *127*, 8618–8626.
(26) Lorieau, J. L.; McDermott, A. E. *J. Am. Chem. Soc.* **2006**, *128*, 11505–11512.
(27) Tjandra, N.; Feller, S. E.; Pastor, R. W.; Bax, A. *J. Am. Chem. Soc.* **1995**, *117*, 12562–12566.
(28) Cornilescu, G.; Marquardt, J. L.; Ottiger, M.; Bax, A. *J. Am. Chem. Soc.* **1998**, *120*, 6836–6837.
(29) Peti, W.; Meiler, J.; Brüschweiler, R.; Griesinger, C. *J. Am. Chem. Soc.* **2002**, *124*, 5822–5833.
(30) Böckmann, A.; Lange, A.; Galinier, A.; Luca, S.; Giraud, N.; Juy, M.; Heise, H.; Montserret, R.; Penin, F.; Baldus, M. *J. Biomol. NMR* **2003**, *27*, 323–339.
(31) Martin, R. W.; Zilm, K. W. *J. Magn. Reson.* **2003**, *165*, 162–174.
(32) Gardiennet, C.; Loquet, A.; Etzkorn, M.; Heise, H.; Baldus, M.; Böckmann, A. *J. Biomol. NMR* **2008**, *40*, 239–250.
(33) Kuszewski, J.; Schwieters, C. D.; Garrett, D. S.; Byrd, R. A.; Tjandra, N.; Clore, G. M. *J. Am. Chem. Soc.* **2004**, *126*, 6258–6273.
(34) Korukottu, J.; Schneider, R.; Vijayan, V.; Lange, A.; Pongs, O.; Becker, S.; Baldus, M.; Zweckstetter, M. *PLoS ONE* **2008**, *3*, e2359.
(35) Andrew, E. R.; Bradbury, A.; Eades, R. G. *Nature* **1958**, *182*, 1659–1659.
(36) Lazar, G. A.; Desjarlais, J. R.; Handel, T. M. *Protein Sci.* **1997**, *6*, 1167–1178.
(37) You, J. X.; Cohen, R. E.; Pickart, C. M. *Biotechnology* **1999**, *27*, 950–954.
(38) Hohwy, M.; Rienstra, C. M.; Jaroniec, C. P.; Griffin, R. G. *J. Chem. Phys.* **1999**, *110*, 7983–7992.
(39) Fung, B. M.; Khitrin, A. K.; Ermolaev, K. *J. Magn. Reson.* **2000**, *142*, 97–101.
(40) Heise, H.; Köhler, F. H.; Xie, X. L. *J. Magn. Reson.* **2001**, *150*, 198–206.
(41) Lange, A.; Luca, S.; Baldus, M. *J. Am. Chem. Soc.* **2002**, *124*, 9704–9705.
(42) Lange, A.; Seidel, K.; Verdier, L.; Luca, S.; Baldus, M. *J. Am. Chem. Soc.* **2003**, *125*, 12640–12648.
(43) Koradi, R.; Billeter, M.; Wüthrich, K. *J. Mol. Graphics* **1996**, *14*, 51.

Values of chemical-shift changes between Ubi-P and microcrystalline preparations using 2-methyl-2,4-pentanediol (MPD) precipitation (referred to as Ubi-M) were determined previously in ref 24, using Ubi-M assignments from ref 44. Summed chemical-shift differences of C′, Cα, and Cβ nuclei were used.

Spin System Simulations. Magnetization transfer in dipolar coupled ^{13}C spin networks under MAS during application of the SPC5 pulse sequence was numerically simulated on the quantum-mechanical (QM) level using the C++ program library GAMMA.[45] A piecewise constant Hamiltonian with a time resolution of 0.09 μs was used, and powder integration over 276 orientations was performed.[46] Spin systems consisted of the two ^{13}C spins involved in the formation of a 2Q state and any ^{13}C spins directly bonded to these, considering isotropic chemical shifts, dipolar and scalar couplings, and spin system geometry. Details of spin system geometries used are given in the Supporting Information. For each spin system, simulations were conducted using dipolar (^{13}C,^{13}C) couplings scaled by order parameters S_{CC} between 0.3 (2- to 4-spin simulations) or 0.5 (5-spin simulations) and 1 in steps of 0.05. Amino acid type-specific simulations were used for ubiquitin, with average chemical shifts taken from BioMagResBank[47] (BMRB). To simulate signal intensities corresponding to cross-peaks in a 2D SPC5 (2Q,1Q) correlation spectrum, the initial density operator was set to $\sum I_z$, and after evolution under the system Hamiltonian H for a time τ corresponding to the duration of the 2Q excitation period (2QE), 2Q coherence between the two spins of interest i, j was projected out from the density matrix using the projection superoperator $\hat{F}_{ij}^{2Q} = |I_+^i I_+^j\rangle\langle I_+^i I_+^j| + |I_-^i I_-^j\rangle\langle I_-^i I_-^j|$ (ref 38). I_z magnetization on spins i and j was then detected after another period τ of evolution under the system Hamiltonian corresponding to double quantum reconversion (2QR).

Analysis of Dynamics. For analysis of cross-peak buildups, (2Q,1Q) correlation spectra were imported in MATLAB (The MathWorks, Natick, MA) using the MatNMR add-on package,[48] and cross-peak volumes were integrated using custom-written scripts. Spectral noise was determined from integrals in noise regions of the same size as cross-peak integrals. After both simulated and experimental buildups were normalized to 1, simulations fitting best to experimental data were determined by calculating the sum of squared differences between simulated and experimental data at the mixing times used for recording (2Q,1Q) spectra. Order parameters given are S_{CC} values used in the simulation yielding the best fit to experimental data, that is, the smallest sum of squared differences between simulated and experimental normalized cross-peak volumes. Errors of order parameters were judged from fitting simulations to experimental data with added noise (as determined from the spectra) and from the range of simulations with different S_{CC} values that fit to experimental data with a root-mean-square deviation (rmsd) differing by no more than 30% from that of the best fit. The error thus determined was usually found to be ±0.05 (i.e., 5%), comparing well to errors of (^{1}H,^{13}C) order parameters in ref 26. This justified running spin system simulations in S_{CC} steps of 0.05. Resultant S_{CC} values are thus always multiples of 0.05 except for 2Q coherences for which best-fitting simulations for the two corresponding cross-peak buildups yielded slightly different S_{CC} values. For these, the average value is given.

(Cα,Cβ) S_{CC} order parameters could be obtained for 40 Ubi-P residues; (Cβ,Cγ), (Cβ,Cγ1), or (Cβ,Cγ2) S_{CC} values were determined for 23 residues (Table SI 1, Supporting Information). (Cα,Cβ) S_{CC} order parameters for three residues (Leu56, Leu67, Leu69) whose signals partly overlap with close sequence neighbors (Leu56 with Asp58; Leu67 with Leu69) were also included in the data set (○ in Figure 4a). Residues without S_{CC} order parameters are either not assigned in Ubi-P, exhibit overlapped resonances in (2Q,1Q) spectra, or are glycine residues lacking side-chain carbons for excitation of (^{13}C,^{13}C) 2Q coherence.

Solution-state NMR order parameters based on backbone (^{1}H,^{15}N) residual dipolar couplings (S_{rdc}^2) were used as published in refs 5, 49 (data set D36M). SsNMR (^{1}H,^{13}C) order parameters measured on Ubi-M (S_{HC}) were taken from ref 26. For comparison with S_{CC} values, S_{HC} values were averaged over the corresponding two ^{13}C nuclei if both values were available. A parameter $\Delta S_{rel,norm}$ was defined as a normalized measure of the relative difference in (Cα,Cβ) S_{HC} and S_{CC} order parameters. For a residue i,

$$\Delta S_{rel,norm}(i) = \frac{|\Delta S_{rel}(i)|}{\max_j(|\Delta S_{rel}(j)|)} \quad (1)$$

with

$$\Delta S_{rel}(i) = (S_{CC}(i) - S_{HC}(i)) - \frac{1}{n}\sum_j (S_{CC}(j) - S_{HC}(j)) \quad (2)$$

with j in eqs 1 and 2 running over all n residues for which both order parameters were available. $\Delta S_{rel,norm}$ is thus independent of an overall offset between S_{HC} and S_{CC} values.

Structure Calculation. For structure calculation, cross-peaks were picked manually in the four Ubi-P CHHC spectra using SPARKY, with minimum contour levels set at 3.5 times the spectral noise level. Folded-in spinning sidebands and diagonal peaks were removed. The PASD algorithm for automated assignment of through-space correlations and structure calculation[33] implemented in Xplor-NIH[50,51] was employed as previously published.[34] Tolerances for matching chemical-shift assignments from ref 24 to CHHC cross-peaks were set to 0.4 ppm, and upper limits for (^{1}H,^{1}H) distance restraints associated with a given CHHC cross-peak assignment were set to 4.0, 5.0, 6.0, or 6.5 Å for peaks from spectra with 62.5, 125, 180, or 250 μs mixing time, respectively, with a common lower distance cutoff of 1.8 Å. Torsion angle restraints derived from Ubi-P assignments using TALOS[52] as well as from NN and NHHC spectra of Ubi-P were used as derived in ref 24. They were enforced using square-well potentials with no energy contribution for deviations within the predicted rmsd.

While three successive passes of PASD structure calculations in torsion angle space were carried out as published,[33,34] final likelihoods of cross-peak assignments were determined with the ubiquitin crystal structure (PDB: 1UBQ) as a reference, effectively using PASD to assign the CHHC spectra with the crystal structure as a search model, similar to the approach used in ref 34. The distance violation cutoff for cross-peak assignments with respect to the reference structure was set to 0.5 Å. The validity of this approach follows from the findings described below and in ref 24 that the Ubi-P structure must be closely related to the crystal structure. 368 unambiguous and 842 ambiguous distance restraints were obtained in this manner, counting also duplicates found in

(44) Igumenova, T. I.; McDermott, A. E.; Zilm, K. W.; Martin, R. W.; Paulson, E. K.; Wand, A. J. *J. Am. Chem. Soc.* **2004**, *126*, 6720–6727.
(45) Smith, S. A.; Levante, T. O.; Meier, B. H.; Ernst, R. R. *J. Magon. Reson., Ser. A* **1994**, *106*, 75–105.
(46) Cheng, V. B.; Suzukawa, H. H.; Wolfsberg, M. *J. Chem. Phys.* **1973**, *59*, 3992–3999.
(47) Ulrich, E. L.; Akutsu, H.; Doreleijers, J. F.; Harano, Y.; Ioannidis, Y. E.; Lin, J.; Livny, M.; Mading, S.; Maziuk, D.; Miller, Z.; Nakatani, E.; Schulte, C. F.; Tolmie, D. E.; Wenger, R. K.; Yao, H.; Markley, J. L. *Nucleic Acids Res.* **2007**, *36*, D402–D408.
(48) van Beek, J. D. *J. Magn. Reson.* **2007**, *187*, 19–26.
(49) Lakomek, N. A.; Walter, K. F. A.; Fares, C.; Lange, O. F.; de Groot, B. L.; Grubmüller, H.; Brüschweiler, R.; Munk, A.; Becker, S.; Meiler, J.; Griesinger, C. *J. Biomol. NMR* **2008**, *41*, 139–155.
(50) Schwieters, C. D.; Kuszewski, J. J.; Clore, G. M. *Prog. NMR Spectrosc.* **2006**, *48*, 47–62.
(51) Schwieters, C. D.; Kuszewski, J. J.; Tjandra, N.; Clore, G. M. *J. Magn. Reson.* **2003**, *160*, 65–73.
(52) Cornilescu, G.; Delaglio, F.; Bax, A. *J. Biomol. NMR* **1999**, *13*, 289–302.

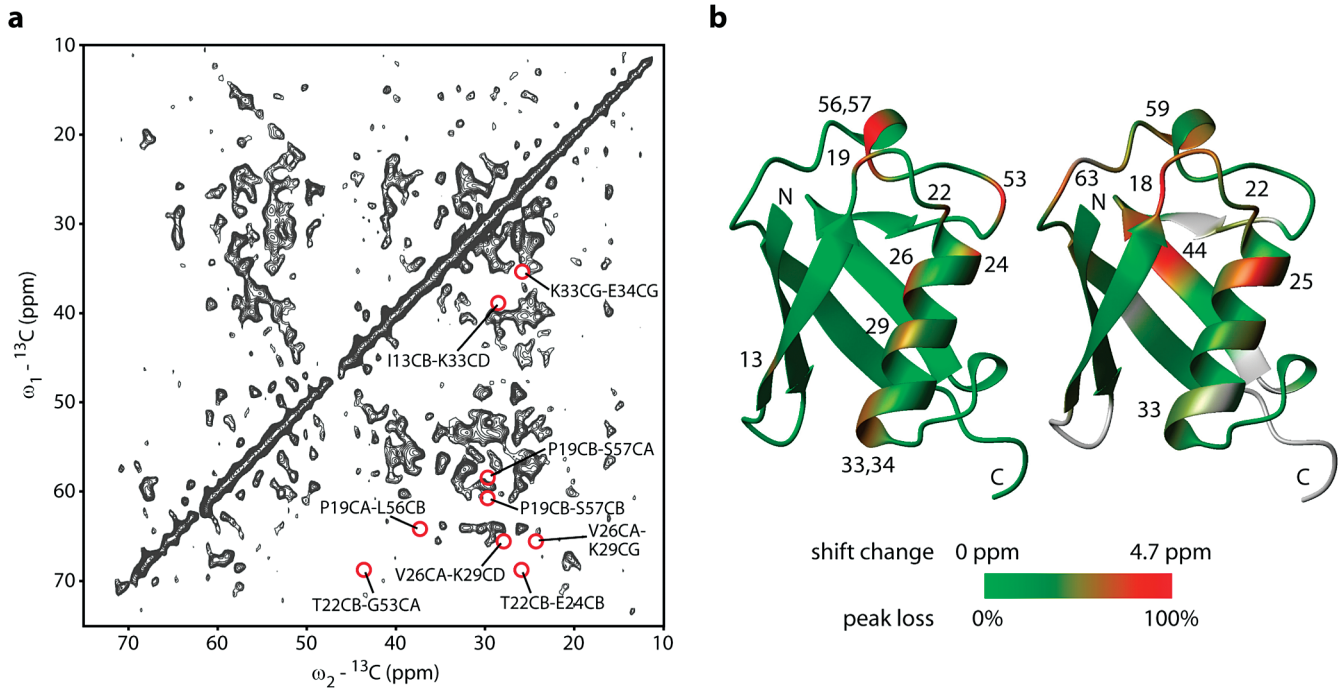

Figure 1. (a) CHHC spectrum of Ubi-P recorded at 14.1 T and 11 kHz MAS with 180 μs (^{1}H,^{1}H) mixing time. Red circles indicate absent inter-residue correlations for nonmethyl carbons that were expected at this mixing time. Associated (^{1}H,^{1}H) distances in the crystal structure are 3.5 Å or less. (b) Color code on the ubiquitin crystal structure (PDB: 1UBQ) indicates the percentage of expected but absent nonmethyl CHHC correlations per residue (left) and summed C′, Cα, and Cβ chemical-shift differences between Ubi-P and Ubi-M as described in ref 24 (right). A brighter red indicates more missing correlations or larger chemical-shift variations, respectively. All residues with absent nonmethyl CHHC correlations (left) and selected residues with large preparation-dependent chemical-shift variations (right) are labeled, as well as the N- and C-termini of the molecule.

more than one spectrum. The unambiguous restraints involved 208 unique (^{13}C,^{13}C) pairs; ambiguous restraints comprised 1186 unique (^{13}C,^{13}C) pairs (Table SI 2, Supporting Information).

Together with the 92 dihedral angle restraints from ref 24, these distance restraints were used for simulated annealing in CNS 1.1 (ref 53). Ambiguous restraints were accounted for by R^{-6} sum averaging over all possible contacts. The simulated annealing protocol used the PARALLHDG5.3 parameter file and started from the crystal structure of ubiquitin (PDB: 1UBQ). Three stages were used: (1) high-temperature annealing in torsion angle space in 1000 time steps of 0.015 ps at 1000 K, (2) very slow cooling in torsion angle space in 10 000 steps of 0.015 ps, reducing the temperature from 1000 K to zero in steps of 50 K, and (3) a final conjugate gradient minimization in 20 cycles of 100 steps each. Force constants were 300, 300, and 150 kcal mol^{-1} Å^{-2} for distance restraints and 100, 200, and 400 kcal mol^{-1} rad^{-2} for dihedral angle restraints in the three stages, respectively. 100 structures were calculated from different initial velocities, of which the 10 structures with lowest overall energy were selected and aligned along the backbone atoms of residues Met1 to Val70 using the program MOLMOL.[43] This software was also used to calculate mean structures of NMR ensembles. Figures of molecular structures were prepared with MOLMOL or PyMOL.[54]

Results and Discussion

Analysis of Ubiquitin CHHC Spectra. Earlier investigations have shown that, in certain regions of the protein sequence, sizable chemical-shift differences occur between different solution- and solid-phase preparations of ubiquitin,[24] pointing to possible preparation-dependent variations in structure or dynamics. In a related approach, we have analyzed the presence or absence of cross signals in CHHC[41,42] through-space correlation spectra of Ubi-P. As a reference structure for this analysis, the ubiquitin crystal structure was used[55] (PDB: 1UBQ), which previous ssNMR studies have indicated to be closely related to the structure(s) present in other solid-phase preparations.[24,25,56] In the initial rate regime, the (^{1}H,^{1}H) distances corresponding to cross-peaks visible in N/CHHC spectra correlate well with the (^{1}H,^{1}H) mixing times used.[32,42] Indeed, a large majority of cross-peaks predicted from the crystal structure was found to be present in CHHC spectra (see Materials and Methods), and a good correlation with mixing time was observed. For unique correlations involving only protons attached to Cα or Cβ nuclei, 86% (49 of 57) of all contacts predicted for (^{1}H,^{1}H) distances up to 2.7 Å are present in a CHHC spectrum with 62.5 μs mixing time, while 93% (84 of 90) of all such contacts up to a (^{1}H,^{1}H) distance of 3.5 Å are found in a CHHC spectrum with 180 μs mixing time. We extended this analysis to all correlations associated with (^{1}H,^{1}H) distances below 3.5 Å for which assignments are available, excluding methyl groups because their polarization is in general weaker if very short CP steps that bracket (^{1}H,^{1}H) mixing are chosen. 186 of 196 (95%) correlations thus predicted are found in the 180 μs CHHC spectrum. This result confirms that valuable distance information can be obtained already from individual N/CHHC spectra and that the structure of Ubi-P must be closely related to the ubiquitin crystal structure.

A closer look at predicted inter-residue correlations, which are absent from the 180 μs Ubi-P CHHC spectrum (red circles

(53) Brunger, A. T.; Adams, P. D.; Clore, G. M.; DeLano, W. L.; Gros, P.; Grosse-Kunstleve, R. W.; Jiang, J. S.; Kuszewski, J.; Nilges, M.; Pannu, N. S.; Read, R. J.; Rice, L. M.; Simonson, T.; Warren, G. L. *Acta Crystallogr., Sect. D* **1998**, *54*, 905–921.
(54) DeLano, W. L. *DeLano Scientific*; Palo Alto, CA, 2002.
(55) Vijay-Kumar, S.; Bugg, C. E.; Cook, W. J. *J. Mol. Biol.* **1987**, *194*, 531–544.
(56) Manolikas, T.; Herrmann, T.; Meier, B. H. *J. Am. Chem. Soc.* **2008**, *130*, 3959–3966.

in Figure 1a, excluding methyl carbons), reveals that the corresponding residues are found in the second β-sheet, the α-helix, and in loop regions around residues 20 and 55 (Figure 1b). Interestingly, these protein regions exhibit substantial chemical-shift changes between Ubi-P and Ubi-M preparations (Figure 1b, see ref 24), indicating a correlation between alterations in ssNMR chemical shift and through-space contacts. It has been suggested that such chemical-shift differences between different solid-phase preparations are most likely to occur in protein regions exhibiting an enhanced degree of molecular mobility.[24] Thus, mobility may also be involved in the attenuation of signals in CHHC spectra.

^{13}C (2Q,1Q) Correlation Spectroscopy as a Measure of Molecular Motion. To investigate whether the observed alterations in ssNMR parameters are due to molecular mobility of the ^{13}C spin network, we explore in the following the use of dipolar (^{13}C,^{13}C) double-quantum correlation spectroscopy. In the context of uniformly ^{13}C-labeled biomolecules, double-quantum recoupling has the advantage that the strongest, that is, one-bond, couplings dominate magnetization transfer,[57] allowing for a local, site-specific description of spin dynamics. In the absence of molecular motion, analytical transfer functions have been given (see, e.g., refs 38, 57) for two- and three-spin systems that take into account the details of the dipolar recoupling sequence under MAS conditions and the relative orientation of the dipolar vectors in the molecular frame. Motion further modulates the orientation-dependent rank 2 components of the anisotropic dipolar interaction[58] and can be represented by a phenomenological order parameter S_{CC} ($0 \le S_{CC} \le 1$) that leads to a scaled effective dipolar coupling d_{CC}^{eff} between two ^{13}C spins i, j as $d_{CC}^{eff} = S_{CC} \cdot d_{CC} = S_{CC} \cdot (\mu_0)/(8\pi^2)(\hbar\gamma_C^2)/(r^3)$ (in units of Hz),[17] with γ_C the gyromagnetic ratio of ^{13}C and r the distance between the two nuclei in question. To relate experimental data to local mobility, we conducted numerical simulations of relevant ^{13}C spin systems using the program package GAMMA[45] and fitted resultant theoretical buildup curves to experimental ones (see Materials and Methods).

First, we verified the approach on the small molecule L-tyrosine-ethylester (TEE, Figure 2a), which exhibits molecular mobility around the ester tail as confirmed by earlier ssNMR studies.[17,21−23] Experimental buildup curves were obtained from a series of (2Q,1Q) correlation spectra recorded on TEE with different 2Q excitation and reconversion times (Figure SI 1, Supporting Information). Simulations were conducted for 2- to 4-spin systems for different values of the order parameter S_{CC}, assuming uniform scaling of S_{CC} for all (^{13}C,^{13}C) dipolar couplings in the spin system. Smaller S_{CC} values, corresponding to larger mobility, reduce the simulated 2Q coherence buildup rate, with strongest variations seen in the initial rate regime (Figure SI 2, Supporting Information). Additional simulations reveal that effects of conformation and chemical-shift anisotropy can be neglected (Figure SI 3, Supporting Information). The broadband character of the dipolar recoupling sequence required us to include in the simulations any ^{13}C spins directly bonded to the two ^{13}C nuclei that contribute to the 2Q coherence (Figure SI 2, Supporting Information), leading to 4-spin simulations in most cases. The fact that neighboring spin−spin couplings alter the polarization transfer dynamics can be appreciated from the analytical expression for cross-peak intensity under SPC5 recoupling in a system of three spins i, j, k given in ref 38. For

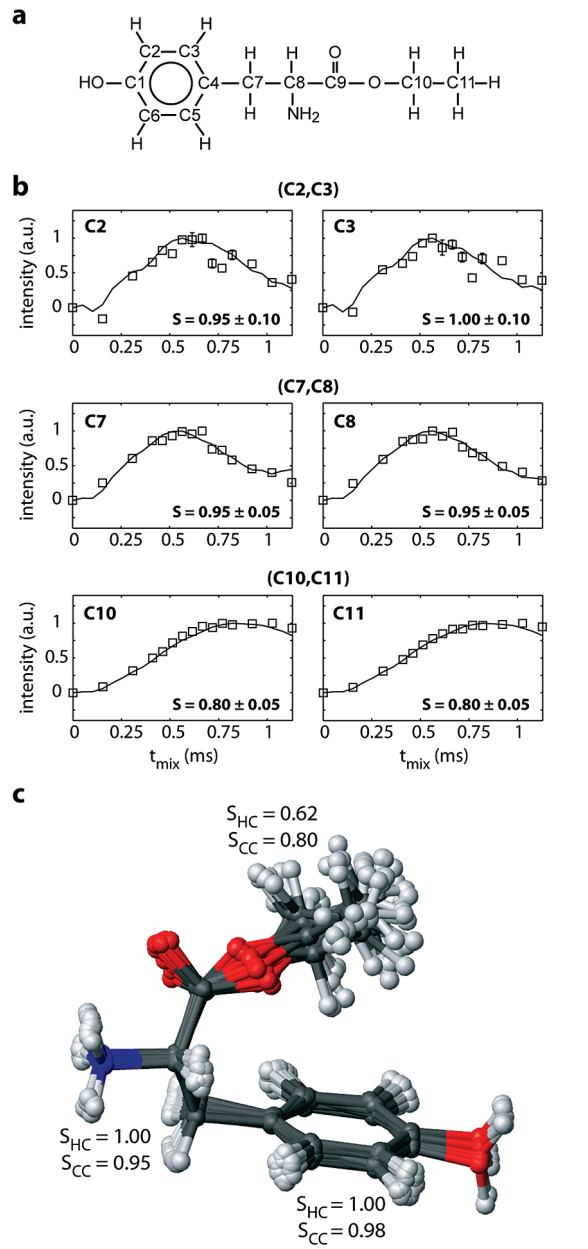

Figure 2. (a) Covalent structure of tyrosine-ethylester (TEE). (b) Experimental 2Q cross-peak buildups (open squares) and best-fitting simulations (lines) for the TEE ^{13}C spin pairs indicated. Order parameters S_{CC} as derived from best fits are given. Error bars are shown where they exceed the size of the data points. (c) Comparison of dipolar (^{1}H,^{13}C) and (^{13}C,^{13}C) order parameters in TEE, both averaged between the two nuclei involved in the 2Q coherences measured (C2 and C3, C7 and C8, and C10 and C11, respectively). (^{1}H,^{13}C) order parameters and the structural ensemble of polycrystalline TEE are reproduced from ref 17.

2Q excitation (2QE) and reconversion (2QR) times of duration τ each, the dominant transfer terms are of the functional form $\cos^2(r\tau)\sin^2(r\tau)$, where r reflects the effective laboratory-frame dipolar coupling $r = \sqrt{(d_{ij,LAB}^2 + d_{jk,LAB}^2 + d_{ik,LAB}^2)}$. This leads to a faster initial buildup as compared to the well-known two-spin limit $\sin^2(d_{ij,LAB} \cdot 2\tau)$ (ref 57).

In Figure 2b, we present experimental 2Q cross-peak volume buildup data for three TEE spin pairs together with best fits from simulations. Within experimental accuracy, all TEE spin pairs except for the (C10,C11) moiety are described by S_{CC} order parameters close to 1, in agreement with previous ssNMR studies of (^{1}H,^{13}C) one-bond couplings.[17,21] On the other hand,

(57) Baldus, M. *Prog. NMR Spectrosc.* **2002**, *41*, 1–47.
(58) Torchia, D. A.; Szabo, A. *J. Magn. Reson.* **1985**, *64*, 135–141.

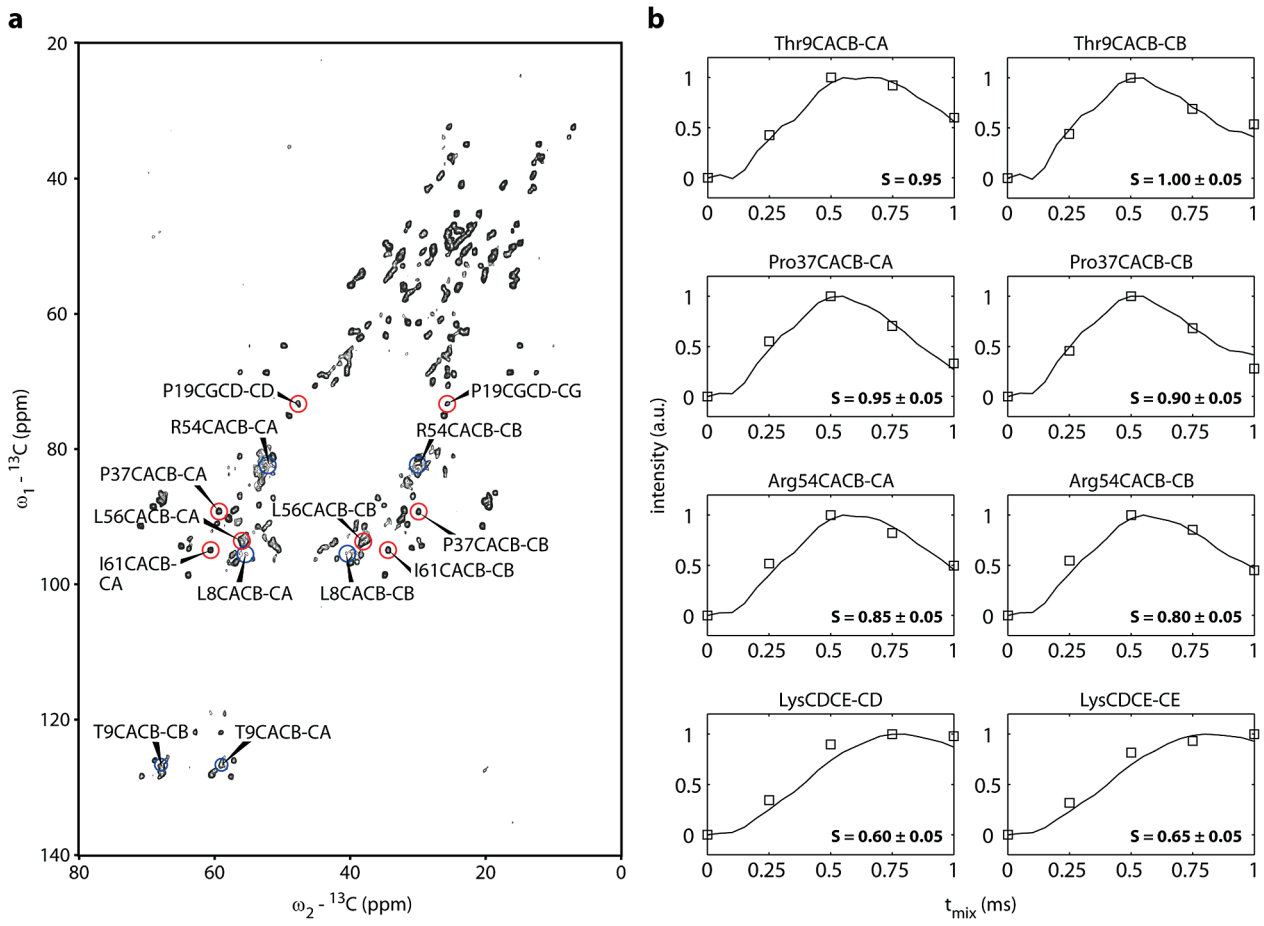

Figure 3. (a) (2Q,1Q) correlation spectrum of Ubi-P recorded at 800 MHz ^{1}H resonance frequency with a 2Q excitation time of 250 μs. Labeled and circled in red are selected resonances clearly present already at this short mixing time, even though they exhibit low order parameters in Ubi-M.[26] Resonances circled in blue are absent in the Ubi-M data set, possibly due to even larger degrees of motion, but present in this spectrum, although of lower signal intensity. (b) Experimental 2Q cross-peak buildups (squares) and best-fitting simulations (lines) for the (Cα,Cβ) nuclei pairs in Thr9, Pro37, and Arg54. Also shown are data and fits for overlapped signals of lysine (Cδ,Cε) nuclei pairs to illustrate the largest degrees of motion observed in our data. S_{CC} order parameters of best-fitting simulations are given with error values. For Thr9 CACB-CA, the error is smaller than 0.05. Error bars of experimental data, calculated on the basis of spectral noise, are smaller than the data points.

the (C10,C11) spin pair is best described by an S_{CC} order parameter of 0.80, indicating elevated mobility of the ester tail. This S_{CC} value is larger than the average of S_{HC} order parameters determined for C10 and C11 (ref 17). This can be expected because S_{HC} should also be sensitive to rotations around the C10−C11 bond, which do not affect the effective (^{13}C,^{13}C) coupling between these two nuclei. S_{CC} and S_{HC} thus probe different modes of molecular motion. Conversely, the fact that S_{CC} is significantly lower than 1 for (C10,C11) indicates that the ester tail exhibits modes of motion in addition to such bond rotation, for example, a nutation as suggested in ref 21.

These results confirm the utility of (^{13}C,^{13}C) double-quantum spectroscopy to probe local molecular dynamics. S_{CC} and S_{HC} order parameters as determined for TEE by ssNMR are summarized in Figure 2c. Comparison with spectra shown in Figure SI 1 (Supporting Information) reveals that a simple intensity analysis of two 2D (2Q,1Q) correlation experiments already provides insight into local molecular mobility, because the (2Q,1Q) cross-peaks of mobile moieties reach maximum intensity only for longer mixing times. However, comparing intensities of different spin systems should be done with caution, because signal intensities can depend on ^{13}C line width or CP transfer efficiency. Considering normalized cross-peak volumes instead of absolute peak heights, as adopted in our quantitative approach, should appropriately account for these factors.

Residue-Specific Dynamics in Ubiquitin. Next, we conducted a series of (^{13}C,^{13}C) 2Q ssNMR experiments on Ubi-P to investigate a possible relation between absent CHHC correlations, chemical-shift changes, and molecular mobility. An existing set of dipolar (^{1}H,^{13}C) order parameters reported for Ubi-M[26] allowed us to also compare dynamical parameters between two microcrystalline preparations.

In Figure 3a, a (2Q,1Q) correlation spectrum of Ubi-P recorded at 800 MHz ^{1}H resonance frequency with 250 μs SPC5 mixing[38] is depicted. Already at this rather short mixing time, several ^{13}C resonances appear in the spectrum that exhibit considerable dynamics according to (^{1}H,^{13}C) order parameters (S_{HC}) reported for Ubi-M.[26] Red circles mark selected pairs of nuclei for which at least one S_{HC} value is below 0.5. Blue circles indicate resonances absent from the S_{HC} data set in ref 26, which has been suggested to be due to even larger mobility of these residues in Ubi-M. These results indicate that differences in protein dynamics between Ubi-P and Ubi-M preparations exist, and we hence carried out a more comprehensive analysis of 2Q buildup data on Ubi-P. Experimental and best-fitting simulated buildup curves for three resonance pairs are shown in Figure 3b. For comparison, data and S_{CC} values for (overlapped) signals of lysine side-chain (Cδ,Cε) pairs are also included that reveal enhanced mobility at the termini of long amino acid side-chains and illustrate the dispersion of S_{CC} order

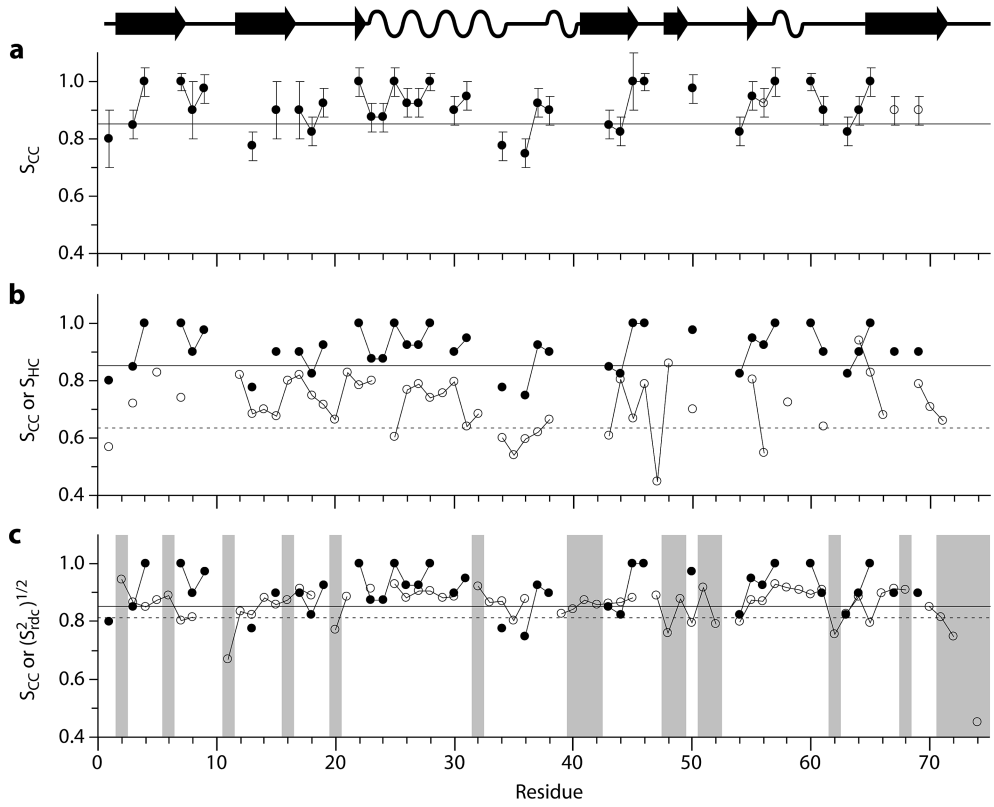

Figure 4. (a) Plot of Ubi-P (Cα,Cβ) S_{CC} order parameters. Open symbols indicate values obtained from signals overlapping with close sequence neighbors. The solid line indicates an S_{CC} value of 0.85 below which the most mobile 20% of determined S_{CC} values are found. Secondary structure of ubiquitin as found in the crystal structure (1UBQ) is sketched at the top. (b) Comparison of Ubi-P (Cα,Cβ) S_{CC} order parameters as in (a) (filled symbols) and Ubi-M S_{HC} order parameters[26] (open symbols). S_{HC} values plotted are averaged over Cα and Cβ nuclei, if both values are available. Solid line as in (a); dotted line denotes the upper limit ($S_{HC} = 0.63$) for the most mobile 20% of residues detected in Ubi-M. (c) Comparison of Ubi-P (Cα,Cβ) S_{CC} values as in (a) (filled symbols) and RDC-based backbone $(S_{rdc}{}^2)^{1/2}$ order parameters from solution-state NMR[49] (open symbols). Solid line as in (a); dotted line ($(S_{rdc}{}^2)^{1/2} = 0.81$) corresponds to the upper limit for the most mobile 20% of residues measured in ref 49. Gray bars indicate residues for which S_{CC} order parameters could not be determined due to weak signal intensity in (2Q,1Q) spectra (Ser20) or due to missing assignments (all other shaded residues).

parameters in Ubi-P. Notably, similar buildup time courses can lead to differing order parameters for different spin systems (compare, e.g., Thr9 and Pro37 in Figure 3b) due to chemical-shift effects. In threonine residues, Cα and Cβ nuclei exhibit larger resonance frequency offsets from the rf carrier we used than in proline, so a slower buildup of magnetization in threonine residues can be expected.

The complete set of S_{CC} order parameters for (Cα,Cβ) pairs we obtained on Ubi-P is shown in Figure 4 a and Table SI 1 (Supporting Information). (Cα,Cβ) S_{CC} order parameters could be determined for 40 residues, that is, 53% of the ubiquitin sequence. In the most mobile 20% of these residues, the (Cα,Cβ) S_{CC} value is below 0.85 (indicated by a solid line in Figure 4a). These residues occur at the N-terminus, in second and third β-strand, and in loop regions. This shows that, also in the PEG-precipitated state, parts of the ubiquitin sequence exhibit considerable dynamics on the ms or faster time scales, comparable to the detected mode of motion of the ester tail in TEE.

Figure 4b compares our Ubi-P S_{CC} order parameters with S_{HC} values measured on Ubi-M.[26] Notably, the same effective sample temperature was used here as in ref 26. Both S_{CC} and S_{HC} values are averaged over Cα and Cβ nuclei to facilitate comparison. The difference of 0.19 between average S_{CC} and S_{HC} order parameters thus obtained (0.91 and 0.72, respectively) is well in line with results obtained on TEE. There, the difference between S_{HC} and S_{CC} values for sites that are not fully rigid, that is, the ester tail, amounts to 0.18. Apart from the overall offset, clear local differences in relative mobility between Ubi-P and Ubi-M data sets are apparent. Especially residues in the loop between the first two β-strands (Leu8, Thr9), in the α-helix (Asn25), and near the 3−10 helix (Leu56) are more rigid in Ubi-P. Notably, loop residues Leu8 and Thr9, which are clearly present in Ubi-P spectra, are absent from the Ubi-M data set, which has been explained by intermediate exchange in these residues in Ubi-M.[26] Interestingly, residues near the short 3-10 helix (consisting of residues Ser57 to Tyr59), where several absent CHHC correlations and larger preparation-dependent chemical-shift changes are found (Figure 1b), are nearly rigid in Ubi-P as seen by their S_{CC} values. Conversely, for example, residues Ile13, Glu18, and Ile44 exhibit larger relative mobility in Ubi-P than in Ubi-M. Different patterns of S_{CC} and S_{HC} order parameters in consecutive residues are also apparent around residues 44, 56, and 64. On the other hand, some common regions of elevated dynamics can be found, most notably at the N-terminus of the molecule and at the end of the α-helix (residues Glu34 to Ile36). Also, while residue Arg54 is rigid enough in Ubi-P to be detected by (2Q,1Q) correlation spectroscopy, it belongs to the most mobile 20% of residues in the Ubi-P data set, consistent with the hypothesis that it is dynamic in Ubi-M.[26]

Residual dipolar couplings (RDCs) between amide protons and nitrogens measured in alignment media in solution-state NMR probe similar time scales of dynamics as the S_{CC} and S_{HC} order parameters discussed so far.[59,60] While experimental and analytical methods are different, as well as the nuclei probed, a recent set of RDC-based (^{1}H,^{15}N) order parameters for

solubilized ubiquitin (further denoted as S_{rdc}^2)[5,49] can be compared to data presented here in terms of the distribution of mobile and rigid residues along the sequence. Figure 4c plots the S_{CC} values we obtained for Ubi-P together with S_{rdc}^2 data for ubiquitin in solution. Square roots of S_{rdc}^2 values are shown for better comparison. Relative to the respective average values, mobility in the N-terminal region up to the α-helix appears more similar between Ubi-M and ubiquitin in solution, with elevated mobility found in residues of the first loop. Ser20, however, is more dynamic in solution (see below). On the other hand, as in Ubi-P, residues in the α-helix (Ile23−Lys33) as well as in the region of the 3−10 helix (Thr55−Ile61) do not seem to exhibit large degrees of dynamics in solution, while some highly dynamic residues are found in these regions in Ubi-M. Notably, a quite similar pattern of S_{rdc}^2 and S_{CC} order parameters is observed in the region between Arg54 and Leu67. Lys48 shows elevated mobility in solution, while its S_{HC} order parameter is one of the largest in the entire Ubi-M data set. However, a "hotspot" of increased dynamics at or around Gly35 at the end of the α-helix appears conserved in all preparations.

Another interesting observation in solution-state S_{rdc}^2 data is that, for several residues that could not be assigned in Ubi-P (Lys11, Lys48, Asp52, Gln62, C-terminal residues) or for which we could not determine S_{CC} order parameters due to lack of intensity in (2Q,1Q) correlation spectra (Ser20; indicated by gray bars in Figure 4c), very low S_{rdc}^2 order parameters are found. While resonance overlap may be involved in missing assignments, this suggests that, in some of these residues, large motional amplitudes may be preserved in PEG microcrystals.

Determination of S_{CC} order parameters was more difficult in side-chain regions due to more extensive resonance overlap and partly weaker signals, leading to less optimal fits. Nevertheless, 23 order parameters were obtained for (Cβ,Cγ), (Cβ,Cγ1), and (Cβ,Cγ2) resonance pairs (see Figure SI 4 and Table SI 1, Supporting Information). In agreement with the expectation to find more mobility in sites more distal from the protein backbone, the average S_{CC} value is lower for (Cβ,Cγ) than for (Cα,Cβ) (0.84 versus 0.91, respectively). The offset from the average Ubi-M S_{HC} value for these sites (0.62) is 0.22 and thus comparable to results for Cα and Cβ nuclei. Interestingly, a better correlation of S_{CC} and S_{HC} order parameters for (Cβ,Cγ) resonance pairs is found than for (Cα,Cβ) (correlation coefficients 0.65 versus 0.27, respectively).

With order parameters for a majority of Ubi-P residues at hand, we could investigate the influence of protein mobility on the absence of CHHC correlations and on preparation-dependent chemical shift changes. In several residues for which expected CHHC correlations are absent, elevated levels of backbone or side-chain mobility are indeed found (Figure SI 5 and Table SI 3, Supporting Information). Figure 5 shows sums of C′, Cα, and Cβ chemical-shift differences between Ubi-P and Ubi-M as determined in ref 24, where the most mobile residues of both preparations as well as those exhibiting the largest relative mobility differences between the preparations (as measured by the parameter $\Delta S_{rel,norm}$, see Materials and Methods and Figure SI 6, Supporting Information) are indicated by red bars. Especially the largest chemical-shift changes can be seen to occur in such mobile or differentially mobile residues. These data thus corroborate earlier hypotheses that molecular mobility is involved in large preparation-dependent chemical-shift differences[24] as well as absent CHHC correlations.[32] However, no strict correlation is observed, because mobility does not necessarily lead to large preparation-dependent chemical-shift changes in a residue (see small red bars in Figure 5). Also, absent through-space correlations are not detected in all of the more mobile residues. This, however, may partly be due to the limits of the approach of identifying absent CHHC cross-peaks. Especially in crowded spectral regions, absent correlations may go unnoticed. Our above argumentation is only based on isolated, clearly identifiable absent cross-peaks (Figure 1a) and can thus be considered a conservative estimate.

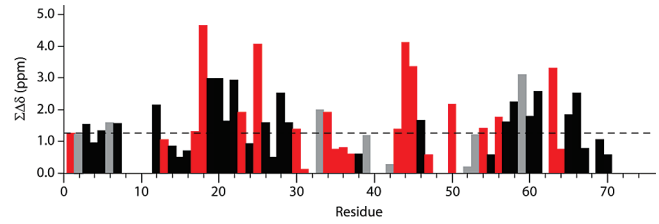

Figure 5. Sum of C′, Cα, and Cβ chemical-shift differences between Ubi-P and Ubi-M as determined in ref 24. Red bars indicate residues with (Cα,Cβ) S_{CC} or S_{HC} order parameters below 0.85 or 0.63, respectively, or with an order parameter difference $\Delta S_{rel,norm}$ at or above the average (see Materials and Methods and Figure SI6, Supporting Information). Gray bars denote residues for which neither S_{CC} nor S_{HC} (Cα,Cβ) order parameters could be determined. Available data for residues with black bars do not indicate elevated mobility or large mobility differences. The dashed line indicates the average Ubi-P−Ubi-M summed chemical-shift difference of 1.25 ppm.

Structure Calculation of Ubi-P. In a number of residues, preparation-dependent chemical-shift changes do not seem to be related to local mobility or mobility differences between Ubi-P and Ubi-M, most notably in residues Pro19−Thr22 and Asp58−Ile61. To investigate whether structural changes play a role instead, a structure calculation of Ubi-P based on the CHHC spectra discussed above was carried out. Four spectra with different (^{1}H,^{1}H) mixing times up to 250 μs were used as input for the automated assignment and structure calculation algorithm PASD implemented in Xplor-NIH.[33,50,51] Similar to the approach described in ref 34, the ubiquitin crystal structure (1UBQ) was used as a search model for CHHC cross-peak assignment. Because of the use of several spectra and looser distance bounds for cross-peak assignment, some restraints were also found that were classified as absent in the above analysis. Restraints obtained in this manner were used for a final simulated annealing step in CNS.[53] The resultant 10 lowest energy structures (Figure 6a) are well converged, with residues 1−70 exhibiting a backbone root-mean-square deviation (rmsd) to the mean of 0.49 Å and of 1.79 Å to the ubiquitin crystal structure (Table SI 2, Supporting Information).

While the structural ensemble is thus well-defined, small but distinct changes are seen with respect to the crystal structure (Figures 6b and SI 7, Supporting Information). Because the rmsd of the Ubi-P ensemble to the crystal structure is larger than its rmsd to the mean, despite the bias toward the crystal structure inherent in our structure calculation protocol, these changes can be considered significant.[34] Deviations in residues for which no assignments and thus no restraints are available cannot be interpreted in terms of structural differences of Ubi-P as compared to the crystal structure. However, other regions for which restraints are available and that are rigid as judged by S_{CC} order parameters indeed appear to assume slightly different conformations in Ubi-P than in single crystals. This is the case for the first loop around residue Leu8 and the 3-10 helix around

(59) Blackledge, M. *Prog. NMR Spectrosc.* **2005**, *46*, 23–61.
(60) Tolman, J. R.; Ruan, K. *Chem. Rev.* **2006**, *106*, 1720–1736.

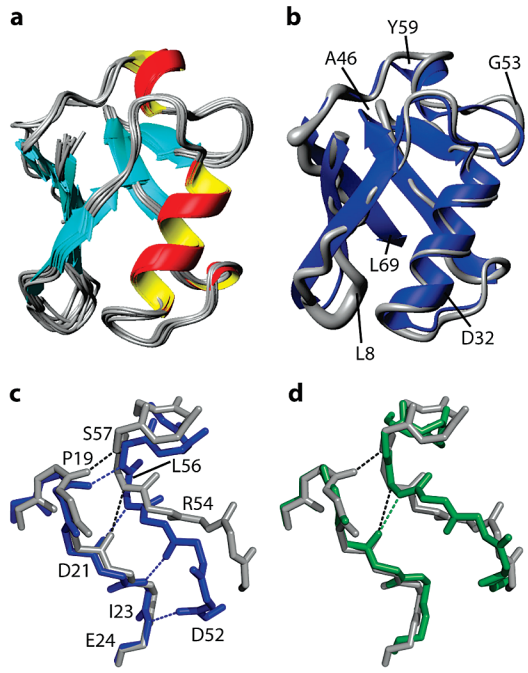

Figure 6. (a) Ensemble of 10 structures with lowest overall energy calculated from 4 CHHC spectra of Ubi-P, using PASD[33] for cross-peak assignment and simulated annealing in CNS.[53] Structures were aligned along the backbone atoms of residues 1−70 using MOLMOL.[43] Only these residues are shown. (b) Sausage plot of residues 1−70 of the ensemble shown in (a) (gray) aligned with the ubiquitin crystal structure (1UBQ, blue). Residues in regions with largest local rmsd deviations between the two structures are labeled. (c,d) Close-up of residues 18−24 and 52−60 in the mean structure of the Ubi-P ensemble (gray, c and d), in the crystal structure (1UBQ, blue, c), and in the mean structure of the Ubi-M ensemble of ref 56 (2JZZ, green, d). Backbone polar contacts as detected by PyMOL[54] are indicated by dashed lines (black for Ubi-P, blue for 1UBQ, green for Ubi-M). Note the absence of a polar contact between residues 19 and 57 in the Ubi-M mean structure.

Asp58. Thus, the preparation-dependent chemical-shift changes and absent CHHC correlations occurring in the latter region appear to be related to local conformational variability.

While analysis of structure and dynamics around residue Leu50 is difficult due to lack of assignments, available evidence suggests that both structural alterations and dynamic processes may play a role here. Flanking residues for which order parameters and/or distance restraints could be obtained exhibit increased dynamics (Arg54) and structural alterations (Ala46, Gly53, Arg54). Elevated dynamics are found in this region also in other ubiquitin preparations.[26,49] Moreover, the largest deviation of a backbone dihedral angle in Ubi-P with respect to the crystal structure is found in residue Arg54 (ref 24), suggesting that the deviation of the calculated Ubi-P structural ensemble from the crystal structure around residue Gly53 indeed reflects a structural alteration of ubiquitin in PEG microcrystals. Conformational changes and increased dynamics in this region likely also affect residues Pro19−Glu24 in the loop between second β-strand and α-helix, which is close in space and partly hydrogen-bonded to residues Asp52−Tyr59 in the ubiquitin crystal structure.[61] This likely explains the preparation-dependent chemical-shift changes and absent CHHC correlations occurring in residues Pro19−Thr22 (Figure 6c,d).

Recently, an ssNMR structure of ubiquitin microcrystals precipitated using MPD was presented[56] (PDB: 2JZZ). Assigned chemical shifts for this preparation, and, consequently, also the pattern of chemical-shift differences to Ubi-P, are very similar to those of Ubi-M (Figure SI 8a, Supporting Information), suggesting that this structure indeed represents Ubi-M as reported in refs 25, 26. As for Ubi-P, the Ubi-M structure is closely similar to the ubiquitin crystal structure, but shows local conformational differences of comparable magnitude (backbone rmsds of the NMR ensembles to the crystal structure are 1.79 and 1.84 Å for residues 1−70 of Ubi-P and Ubi-M, respectively). The mean structures of the Ubi-P and Ubi-M ensembles differ from each other by a backbone rmsd of 2.22 Å (residues 1−70). This value is clearly larger than the rmsds of the structural ensembles to their respective mean (0.49 and 0.87 Å for residues 1−70 of the 10 lowest energy structures in the Ubi-P and Ubi-M ensembles, respectively), in line with the notion that the two sample preparations lead to conformational differences in ubiquitin (Figure SI 8b,c, Supporting Information). Apart from differences in the unrestrained C-terminus and in residues 8−12, 31−32, and 39, which are unassigned or next to unassigned residues in one or both data sets, the largest conformational changes between Ubi-P and Ubi-M are seen in regions where the preceding discussion has already indicated dynamical and/or structural differences between the preparations (around residues 46, 54, and 64). Notably, many large chemical-shift changes especially in the N-terminal part of the protein do not coincide with structural differences, but rather occur in mobile or differentially mobile residues (e.g., residues 18, 25, 34), further supporting the role of molecular dynamics in the origin of chemical-shift differences.

Additional Motional Processes and the Influence of Intermolecular Interactions. S_{CC} order parameters determined here do not cover all motional time scales, and other dynamic processes may be present in microcrystalline ubiquitin. For example, for several residues in ubiquitin in solution, slow exchange processes on a microsecond to millisecond time scale have been reported, particularly for residues Ile23−Asn25 and Glu51−Gly53 (refs 27, 61, 62), but also residues Thr9, Glu18, Ile30, Lys33, Ile36, Leu43, Phe45, Thr55−Asp58, and Val70 have been implicated in slow dynamic processes.[61] For many of these residues, available S_{CC} order parameters do not point to elevated mobility, with the exception of Glu18, Ile36, Leu43, and possibly Glu51−Gly53. Slow exchange in the other residues thus appears to be absent in Ubi-P or to occur on time scales slower than detectable by 2Q (^{13}C,^{13}C) spectroscopy. Such slow conformational exchange may also account for peak doubling observed in several residues of Ubi-P that do not exhibit high mobility on the S_{CC} time scale, that is, residues Thr9, Ile23, Val26, Pro37, and Ala46.[24] However, intermolecular packing effects may limit the motional degrees of freedom in Ubi-P. In solution, a correlation of local mobility in ubiquitin with exposure of amino acid side-chains to the solvent has been observed.[63] In Ubi-P, however, no correlation of S_{CC} order parameters and fractional accessible surface area of individual residues could be found (see Figure SI 9, Supporting Information). This may reflect the fact that in microcrystals, in contrast to the solution state, the surface of the protein faces not only solvent, but also precipitant and neighboring molecules. Indeed, assuming local packing of molecules similar as in single crystals, a variety of intermolecular contacts are predicted (Figure SI 10, Supporting Information) with local minima found in protein regions characteristic for large changes in ssNMR shifts or

(61) Massi, F.; Grey, M. J.; Palmer, A. G. *Protein Sci.* **2005**, *14*, 735–742.
(62) Majumdar, A.; Ghose, R. *J. Biomol. NMR* **2004**, *28*, 213–227.
(63) Lakomek, N. A.; Fares, C.; Becker, S.; Carlomagno, T.; Meiler, J.; Griesinger, C. *Angew. Chem., Int. Ed.* **2005**, *44*, 7776–7778.

dynamics (Figure 5). On the other hand, large numbers of crystal contacts are seen for residues Pro19, Ser20, Gly35, Arg54, Lys63, and the C-terminus. Hence, a direct correlation between intermolecular interactions and elevated dynamics and/or chemical-shift changes cannot be established. This may partly be due to intrinsic limitations in terms of both protein populations and motional rates that can be detected by 2Q ssNMR spectroscopy.

Considering residues 1−70, average (Cα,Cβ) S_{CC} and solution-state $(S_{rdc}^2)^{1/2}$ order parameters of 0.91 and 0.86, respectively, appear to indicate comparable overall backbone dynamics, with predominantly higher values seen in the solid state. The average Ubi-M S_{HC} value in these residues, averaged over Cα and Cβ nuclei, is 0.72 and thus considerably lower. As mentioned, in ubiquitin, the offset of S_{HC} and S_{CC} values averaged over Cα and Cβ nuclei is similar to that found for the ester tail in TEE, where the lower S_{HC} value may be explained by rotational motion around the C−C bond. If only ubiquitin Cα S_{HC} values are compared to (Cα,Cβ) S_{CC} data, this overall offset decreases but still remains significant (0.78 vs 0.91, $p < 0.001$, one-sided t test). One possible motional model to explain this difference could be a nutation of the Hα−Cα bond vector around its main direction, that is, a diffusion in a cone similar to that postulated for the TEE ester tail.[21,64] (Cα,Cβ) order parameters larger than corresponding (Hα,Cα) values would then indicate that such motion is less pronounced in the Cα−Cβ bond, possibly due to steric restraints imposed by the other atoms bound to Cβ. On the other hand, overall backbone dynamics may simply be higher in Ubi-M than in the Ubi-P preparation. However, apart from the nuclei involved, also the recoupling sequences and associated effective dipolar coupling elements used for determination of S_{CC} and S_{HC} values are different. Absolute order parameter values from different experiments should thus be compared with caution. This work consequently focused on relative mobility differences in individual protein regions, with respect to the average order parameters found in each data set.

Recent studies have suggested that motions on time scales detected by measurements of dipolar couplings and exchange effects in solution occur in ubiquitin residues involved in protein−protein interactions.[5,61,62] This correlation is most pronounced for the exposed loop in residues Thr7−Lys11 and the ubiquitin "interaction surface" between residues Gln40 and Leu50, although not for all residues a perfect correlation is seen. In particular, some residues crucial for protein−protein interactions are rather rigid in solution (Ile44, His68).[5,65] As far as assignments and S_{CC} values are available, the first loop is quite rigid in Ubi-P, however. On the other hand, enhanced dynamics can be detected in Ubi-P residues between Gln40 and Leu50 (Leu43, Ile44) or may be present in others that could not be assigned or analyzed in (2Q,1Q) correlation spectra. Notably, key residues known to be involved in interactions with ubiquitin-binding domains (Ile44), E1 enzymes (Ile44, Arg54), and in polyubiquitination (Lys63) appear among the most dynamic 20% of residues for which S_{CC} values could be obtained. This agrees with recent findings that free ubiquitin dynamically samples the conformations it assumes in complex with different interacting proteins, that is, that conformational selection appears to govern interactions of ubiquitin with other proteins.[5]

Conclusions

We have shown that 2Q (^{13}C,^{13}C) ssNMR spectroscopy represents a sensitive means to detect dynamics of solid-phase biomolecules at the atomic scale. In the initial rate regime, the signal amplitude in (2Q,1Q) correlation experiments is strongly modulated by molecular motion. Especially when the recording of entire three-dimensional data sets is prohibited by spectroscopic sensitivity, the approach outlined here may provide a useful means to identify molecular regions of enhanced mobility in a small number of 2D experiments. Simulations and data fitting procedures were developed to analyze polarization transfer dynamics quantitatively. Data obtained on the test system TEE are in good agreement with previous ssNMR order parameter measurements, showing a rigid molecule except for the ethyl ester tail, which exhibits correlated motion.

Application of our approach to microcrystalline ubiquitin reveals that, similar to that in solution and in MPD microcrystals, ubiquitin precipitated from PEG exhibits sizable mobility on the time scales detected by one-bond (^{13}C,^{13}C) dipolar couplings. While common regions of elevated dynamics can be found in all preparations, the detailed distribution of mobile and rigid residues appears to be distinctly preparation-dependent. In particular, ubiquitin motion in PEG microcrystals differs from that seen in MPD-precipitated ubiquitin, offering an explanation for several large preparation-dependent chemical-shift changes and absent CHHC correlations.[24] Structure calculation indicated conformational changes in loop regions of PEG-precipitated ubiquitin with respect to the crystal structure and MPD-precipitated ubiquitin, accounting for most other observed sizable chemical-shift changes and absent through-space correlations.

Chemical-shift variations in ssNMR are commonly linked to polymorphism and are widely occurring in small molecules,[66] microcrystalline proteins such as discussed here or amyloid fibrils.[67,68] Our results on ubiquitin reveal that the origin of such phenomena may, at least in part, be related to molecular dynamics, even in a crystalline lattice. In a broader sense, the approach described here should hence be useful for other ssNMR-based biomolecular studies, for example, involving membrane proteins, protein fibrils, and other biomolecular complexes in a heterogeneous molecular environment. Increasing evidence suggests that, in these systems, molecular dynamics and intermolecular interactions play a crucial role for molecular organization and function in membranes[14,69] or in a cellular[70] context.

Acknowledgment. Technical assistance by K. Giller and B. Angerstein and financial support by a Ph.D. fellowship to R.S. by the DFG graduate school 782 "Spectroscopy and Dynamics of Molecular Coils and Aggregates" is gratefully acknowledged. We

(64) Palmer, A. G. *Chem. Rev.* **2004**, *104*, 3623–3640.
(65) Hicke, L.; Schubert, H. L.; Hill, C. P. *Nat. Rev. Mol. Cell Biol.* **2005**, *6*, 610–621.
(66) Harris, R. K. *Analyst* **2006**, *131*, 351–373.
(67) Heise, H.; Hoyer, W.; Becker, S.; Andronesi, O. C.; Riedel, D.; Baldus, M. *Proc. Natl. Acad. Sci. U.S.A.* **2005**, *102*, 15871–15876.
(68) van der Wel, P. C. A.; Lewandowski, J. R.; Griffin, R. G. *J. Am. Chem. Soc.* **2007**, *129*, 5117–5130.
(69) Etzkorn, M.; Kneuper, H.; Dunnwald, P.; Vijayan, V.; Kramer, J.; Griesinger, C.; Becker, S.; Unden, G.; Baldus, M. *Nat. Struct. Mol. Biol.* **2008**, *15*, 1031–1039.
(70) Inomata, K.; Ohno, A.; Tochio, H.; Isogai, S.; Tenno, T.; Nakase, I.; Takeuchi, T.; Futaki, S.; Ito, Y.; Hiroaki, H.; Shirakawa, M. *Nature* **2009**, *458*, 106–U11.

thank Nils Lakomek and Christian Griesinger for providing solution-state NMR order parameters of ubiquitin.

Supporting Information Available: Details of spin system simulations; TEE (2Q,1Q) correlation spectra; simulations of signal evolution in (2Q,1Q) correlation spectra for different order parameters, spin system geometries, and chemical-shift anisotropies; plot of Ubi-P (Cβ,Cγ) S_{CC} order parameters; plot of absent Ubi-P through-space correlations; combined plot of S_{CC} and S_{HC} order parameters, normalized order parameter differences, and chemical-shift changes; plots of rmsd and number of restraints per residue for calculated Ubi-P structures; chemical-shift and structural differences between Ubi-M as published in ref 56 and Ubi-P; plots of fractional accessible surface area and crystal contacts per residue in the ubiquitin crystal structure; list of Ubi-P (Cα,Cβ) and (Cβ,Cγ) S_{CC} order parameters; structural statistics for calculated Ubi-P structures; and list of absent Ubi-P through-space correlations. This material is available free of charge via the Internet at http://pubs.acs.org.

JA906283H